

## Temperature Controlled Voltage Oscillation in Neural Circuit Undergoing Homoclinic Bifurcation

Yasuomi D. Sato

\*Department of Brain Science and Systems Engineering, Graduate School of Life Science and Systems Engineering, Kyushu Institute of Technology, Japan

\*\* Frankfurt Institute for Advanced Studies (FIAS), Goethe University Frankfurt, Germany

**ABSTRACT:** We analyze a frequency decrease as well as a frequency transition with a temperature increase in the Hodgkin-Huxley (HH) oscillator undergoing saddle homoclinic bifurcations. A gradient of frequency for temperature is derived by perturbation analysis of the stable HH oscillators, in combination with the other gradient of frequency for input current and a so-called phase response curve (PRC) multiplied by its related voltage-gated channel currents. We then show that the PRC is clearly classified by the gradient of frequency for temperature. More interestingly, different bifurcation mechanisms of the Andronov-Hopf and the saddle-node are commonly categorized.

**Keywords:** Hodgkin-Huxley oscillator, frequency decrease, oscillatory transition, saddle homoclinic orbit bifurcation, phase response curve

### I. INTRODUCTION

Temperature is one of important physical variables, which significantly affects autonomous oscillations generated in the nervous system. Gamma oscillations evoked on rat hippocampal slices are dependent of temperature [1]. In simulations on models of the nervous system, temperature alters nonlinear phenomena of desynchronization or chaos synchronization in the voltage activities [2][3]. It is thus interesting to understand mechanisms on emergences of the oscillation, which are subject to temperature variation, or to study temperature effects on cooperative behavior in the neural network.

Mathematical analysis on voltage oscillations in a single neuron is fundamental for understanding collective behavior in the assemblies. The Hodgkin-Huxley (HH) model is the first mathematical description on such voltage dynamics. The HH model can describes how membrane potentials in neurons are initiated and propagated [4]. It is modified for simulating peripheral cold receptors discharges that exhibit different firing patterns [5]. One firing pattern is an abrupt increase of the interspike intervals in a certain temperature region. This is originated from a homoclinic bifurcation of a saddle-node (SN) equilibrium embedded in the chaotic attractors [6]. However, why the homoclinic bifurcation appears is still unclear. The modified HH model seems to be different from the original. We will have to study again stability analysis on equilibriums in both the original and modified HH models.

It is also necessary for us to find another measurement for characterizing firing properties or dynamical mechanisms in their models. The good measurement is the frequency-current ( $f-I$ ) curve [7], which has already been examined in electrophysiological experiments [8][9]. The  $f-I$  curve generally categorizes oscillations into the two classes: For the class I, emergence of the oscillation with zero frequency is characterized by saddle-node (SN) or saddle-node on invariant circle (SNIC) bifurcations with an increase of the  $I$ . The SNIC, which is also called the SN on a limit cycle (SNLC), means that the SN bifurcation occurs on the LC. In the class II, emergence of the oscillation with a finite frequency is characterized by the Andronov-Hopf (AH) bifurcation.

In recent analysis, one unexpected oscillatory phenomenon has been highlighted that the class I Morris-Lecar (ML) model decreases firing frequency with temperature increase [10]. This seems to be very similar to frequency discharge of cold fibers, which also shows the paradoxical frequency discharge at high temperature [11][12] (In what follows, let us call it the frequency transition). In 1999, Adair simulated the frequency discharge of cold fibers by Boltzmann description of voltage-gated  $\text{Na}^+$  and  $\text{Ca}^{2+}$  channels [13]. Presumably, this Boltzmann model is not functionally different from the original HH model. However, using the original HH model, how the paradoxical frequency discharge occurs is still unclear. It should thus be clarified by analyzing stabilities as well as bifurcation mechanisms in the original HH model.

In this paper, we show that temperature ( $\mu$ ) modulated frequency are characterized with current  $I$  and so-called phase response curves (PRCs) derived by making phase descriptions for small  $\mu$  perturbation.  $f-\mu$  formulations give us mathematical conditions for a frequency decrease and a frequency transition with an increase in temperature, dependent of different bifurcation mechanisms on oscillation generation. Frequency gradients in terms of  $\mu$  classify PRC into two types, regardless of conventional classification. We demonstrate heuristically firing frequency transition for larger  $\mu$  in the HH model undergoing a SNIC bifurcation mechanism. Also, a frequency increase with a  $\mu$  decrease is determined by appropriate proportion of frequency gradient for  $I$  to the product of the PRC and its current dynamics. In addition, the frequency gradient in terms of  $\mu$  shows the critical  $\mu$ -value for the frequency transition of a normal saddle-node homoclinic orbit to its separatrix loop. Finally, discussion and conclusion will be given.

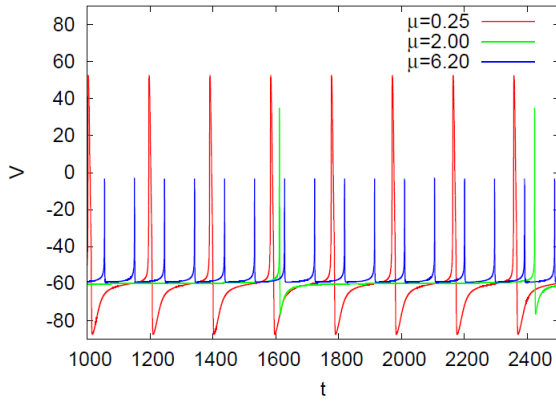


Fig. 1. Dynamics for the Hodgkin-Huxley (HH) neuron model at  $I = 0.161$ , parameterized as class I. The time courses of the membrane voltage when  $\mu$  increases from 0.25 to 6.2 via 2.

## II. BIFURCATIONS IN SPIKING MODEL

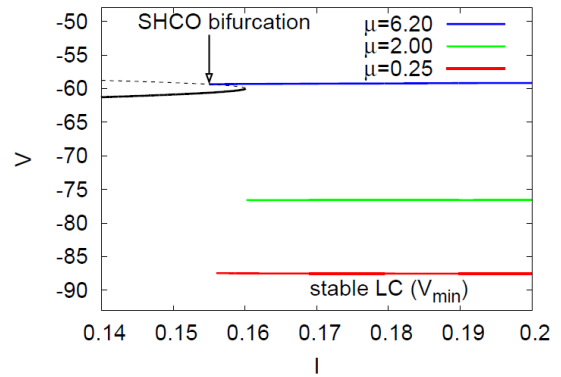
We shall begin by studying bifurcation analysis on the Hodgkin-Huxley (HH) model parameterized as a class I. The HH model, which is employed to simulate frequency-current ( $f-I$ ) and frequency-temperature ( $f-\mu$ ) relations, is given by

$$C_m \frac{dV}{dt} = Q(V, m, h, n) + I = -g_{Na} m^3 h (V - E_{Na}) - g_K n^4 (V - E_K) - g_L (V - E_L) + I, \quad (1)$$

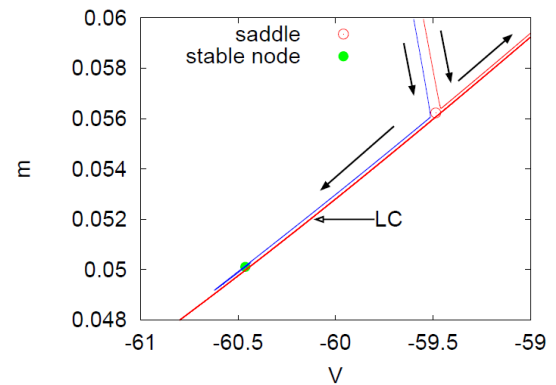
$$\frac{dy}{dt} = \mu P_y(V, y) = \mu (Y_\infty(V) - y) / \tau_y(V). \quad (2)$$

$C_m (= 1\mu F/cm^2)$  is the membrane capacity.  $y \in \{m, n, h\}$  is the non-dimensional gating variable. The parameters  $E_{Na}$ ,  $E_K$ , and  $E_L$  are the reversal potentials of  $Na^+$ ,  $K^+$  and leak currents respectively, while  $g_{Na}$ ,  $g_K$ , and  $g_L$  are the conductances.  $Y_\infty(V) = \alpha_y(V) / (\alpha_y(V) + \beta_y(V))$ ,  $\tau_y(V) = 1 / (\alpha_y(V) + \beta_y(V))$  where  $\alpha_m(V) = -0.1(V + V_1) / (\exp(-0.1(V + V_1)) - 1)$ ,  $\beta_m(V) = 4\exp(-(V + V_2) / 18)$ ,  $\alpha_h(V) = 0.07\exp(-(V + V_3) / 20)$ ,  $\beta_h(V) = 1 / (\exp(-0.1(V + V_4)) + 1)$ ,  $\alpha_n(V) = 0.01(V + V_5) / (\exp(-0.1(V + V_5)) - 1)$  and  $\beta_n(V) = 0.125\exp(-(V + V_6) / 18)$ . The class I dynamics are parameterized with  $g_{Na} = 35 \text{ mS/cm}^2$ ,  $E_{Na} = 55 \text{ mV}$ ,  $g_K = 9 \text{ mS/cm}^2$ ,  $E_K = -90 \text{ mV}$ ,  $g_L = 0.1 \text{ mS/cm}^2$ ,  $E_L = -65 \text{ mV}$ ,  $V_1 = 35$ ,  $V_2 = 60$ ,  $V_3 = 58$ ,  $V_4 = 28$ ,  $V_5 = 34$  and  $V_6 = 44$  (see [2]) so that the HH model represents an oscillatory system exhibiting repetitive firings via a saddle homoclinic orbit (SHCO) bifurcation with the current increase (see Fig. 1). The detailed bifurcation mechanism will be examined below. As shown in Fig. 1, firing frequency of oscillation decreases and then increases again, and its amplitude of oscillation monotonically decreases when  $\mu$  increases.

We study dynamical mechanisms underlying changes of firing frequency with a temperature increase by analyzing stabilities of stationary solutions of the HH model. The result is shown in Fig. 2(a). For any  $\mu$ , a saddle and stable nodes coexist for  $I < I_{SN}$  ( $=0.16$ ). Their stabilities are numerically calculated as referred in [14][15].  $I_{SN}$  is saddle-node (SN) equilibrium. Trajectories, which diverge from the unstable node and the saddle, converge to the stable node (not shown here). When  $I$  exceeds 0.152 for  $\mu=0.25$ , a stable LC attractor appears through a SHCO bifurcation so that the attractor exists together with the stable node. Since trajectories on the LC attractor pass outside the saddle and stable node on the  $V-m$  phase plane,



(a)

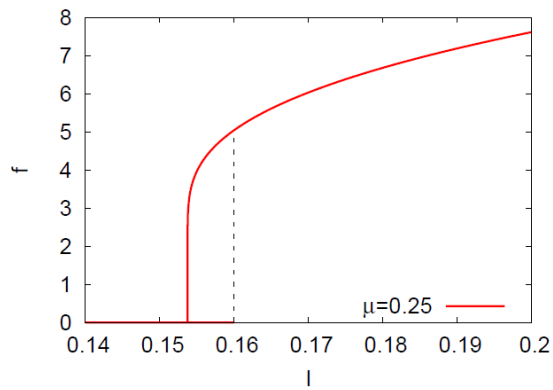


(b)

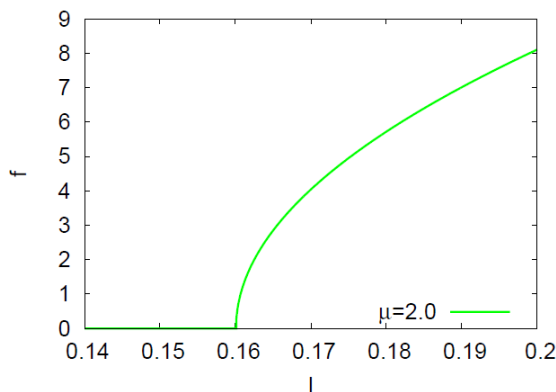
the LC can be called as the big homoclinic orbit (Fig. 2(b)). The LC attractor still remains even if  $I > I_{SN}$ . This indicates emergences of the oscillation via two different bifurcation mechanisms: The first oscillation with 0-frequency occurs via the SHCO bifurcation. The second oscillation with a finite frequency occurs via the SN bifurcation [Fig. 3(a)]. We notice that the second oscillation emergence is slightly different from the typical one via the SN bifurcation.

Next we show that for  $\mu=2$ , the HH model begins oscillations with 0-frequency through the SN bifurcation as shown in Figs. 2(a) and 3(b). We cannot find any bi-stability state of the node and the LC attractor as shown in Fig. 3(a). To be more precise, such a SN bifurcation is called the SN on invariant cycle (SNIC) as referred to [7]. This means SN equilibrium occurs on a LC attractor. Here notices that a size of the LC is apparently reduced as in the increased  $V_{min}$  of Fig. 2(a).

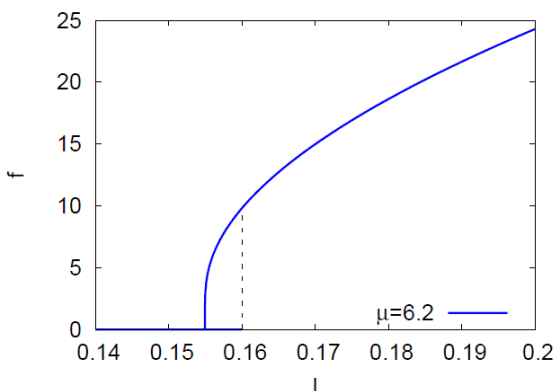
Finally, we can see again a SHCO bifurcation when  $\mu=6.2$  [Fig. 2(a)]. This is a slightly different from the case for  $\mu=0.25$ , in terms of whether or not the SN equilibrium is



(a)



(b)



(c)

Fig. 3.  $f$ - $I$  curves for  $\mu = 0.25, 2$  and  $6.2$ . The HH model ((a)  $\mu = 0.25$  and (c)  $\mu = 6.2$ ) begins class II oscillations via the SN bifurcation while terminating the oscillations in the class I. (b) The HH model ( $\mu = 2$ ) shows simultaneous excitabilities and oscillations of the class I.

outside of the homoclinic orbit. We show again the  $f$ - $I$  curve with the bi-stability (see Fig. 3(c)). Because the trajectory is attracted into the HCO, the amplitude as well as the frequency of the oscillation is respectively small and high as shown in Fig. 1.

In summary, we find  $f$ - $\mu$  relation at each current level as shown in Fig. 4. Before a SN bifurcation, the frequency is in small peak for  $\mu < 0.5$  while its frequency slope for  $\mu > 6.0$  is extremely sharp. Immediately after the SN bifurcation, a constant low frequency level appears in the middle range of  $\mu$ . It gradually increases as  $I$  increases from  $I_{SN}$ . The  $f$ - $\mu$  curve then becomes a monotonic increasing curve for temperature. This indicates that a

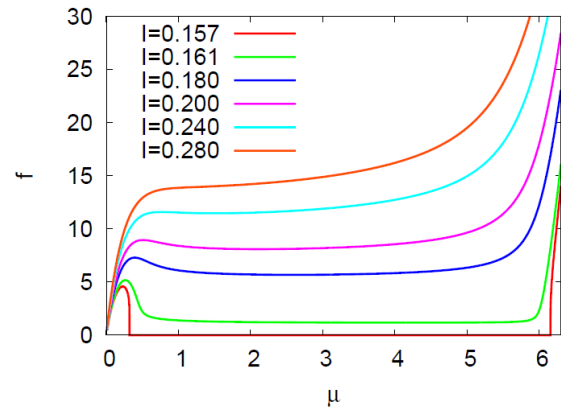


Fig. 4. Frequency  $f$  versus temperature  $\mu$  on simulation with the class I HH neuron model. When  $I=0.161$ , the frequency passed through a minimum for  $\mu=6$  and then extremely increased at the higher temperature. The low frequency level gradually rises so that the frequency is a monotonically increasing function of temperature.

frequency decrease and a frequency transition with a temperature increase are based on two SHCO bifurcation mechanisms for  $\mu < 0.5$  and  $\mu > 6.0$  around the SN equilibrium.

### III. PERTURBATION APPROACHES

Next, in order to deepen more understandings of the frequency decrease and frequency transition, we employ a phase reduction method [10][16][17][18]. In the phase reduction method, reducing  $n$ -dimensional oscillatory dynamics, subject to small perturbations of temperature and current ( $\Delta\mu$  and  $\Delta I$ ), to the one-dimensional phase equation, the perturbations are even phase-described. Then, we find that frequency gradient for temperature ( $[\partial f / \partial \mu]$ ) is related to another oscillatory property such as PRCs and  $f$ - $I$  curves.

The HH oscillator perturbed with small temperature and small current is written in the general form:

$$\frac{dx}{d\tau} = \mathbf{F}(\mathbf{x}) + \mathbf{G}(\mathbf{x}), \quad (3)$$

where  $\mathbf{x}=(V, \mathbf{y}) \in \mathbb{R}^4$ .  $V$  is the potential variable while  $\mathbf{y}$  is a vector consisting of 3 recovery variables.  $\mathbf{F}(\mathbf{x})$  is a vector field ( $Q(\mathbf{x}) + I_0, \mu_0 \mathbf{P}(\mathbf{x})$ ) where  $Q$  is the membrane potential dynamics for  $V$ .  $\mathbf{P}(\mathbf{x})$  is the recovery dynamics for  $\mathbf{y}$ . The perturbation term  $\mathbf{G}(\mathbf{x}) = (\Delta I, \mathbf{P}(\mathbf{x}) \Delta\mu)$ .

Let  $\mathbf{x}_p(\tau)$  denote the unique phase asymptotically stable  $T_p$ -periodic function to

$$\frac{d\mathbf{x}_p}{d\tau} = \mathbf{F}(\mathbf{x}_p). \quad (4)$$

where  $\mathbf{x}_p(\tau + T_p) = \mathbf{x}_p(\tau)$ . Then a stable solution for Eq. (3) is approximated as

$$\mathbf{x}(\tau) = \mathbf{x}_p(\tau + \eta(\tau)) + \mathbf{u}(\tau + \eta(\tau)), \quad (5)$$

where  $\eta(\tau)$  means a small perturbation in the phase direction on the periodic orbit.  $\mathbf{u}(\tau + \eta(\tau))$  denotes the orbital deviation to the periodic orbit  $\mathbf{x}_p(\tau)$ . Substituting Eq. (5) into Eq. (3) and expanding the both-hand sides into a Taylor series leads

$$\left[ \dot{\eta}(\tau) \frac{dx_p(q)}{dq} + \frac{d}{dq} \mathbf{u}(q) \right]_{q=\tau+\eta(\tau)} = \frac{\partial \mathbf{F}(x_p(\tau+\eta(\tau)))}{\partial \mathbf{x}} \mathbf{u}(\tau + \eta\tau + \mathbf{G}\mathbf{x}_p\tau + \eta\tau. \tag{6}$$

In the perturbed oscillator, the orbital deviation vector  $\mathbf{u}(\tau) = \mathbf{x}(\tau) - \mathbf{x}_p(\tau)$  evolves as  $[d\mathbf{u}(\tau)/d\tau] = [\partial \mathbf{F}(x_p(\tau))/\partial \mathbf{x}] \mathbf{u}(\tau)$ . The vector  $\mathbf{Z}(\tau)$  tangent to the periodic orbit  $\mathbf{x}_p(\tau)$ , which is the unique solution to

$$\frac{d\mathbf{Z}}{d\tau} = - \left[ \frac{\partial \mathbf{F}(x_p)}{\partial \mathbf{x}} \right]^t \mathbf{Z}, \tag{7}$$

where  $^t$  is transpose and the normalization condition

$$\mathbf{Z} \cdot \frac{d\mathbf{x}_p}{d\tau} = 1 \tag{8}$$

is satisfied for every  $\tau$ .  $\mathbf{Z}(\tau)$  is the adjoint solution to the linearization around the limit cycle. The first element of the adjoint solution,  $Z_V(\tau)$ , is the PRC widely used in computational neuroscience. Eq. (3) is then reduced to the evolution equation for  $\eta$ :

$$\dot{\eta}(\tau) = \mathbf{Z}(\tau + \eta(\tau))^t \cdot \mathbf{G}(\mathbf{x}_p(\tau + \eta(\tau))). \tag{9}$$

Introducing phase variables defined by  $\theta = (\tau + \eta) / T_p$  ( $\in [0, 1)$ ), Eq. (9) is rewritten as

$$\frac{d\theta}{d\tau} = \frac{1}{T_p} + \frac{1}{T_p} \int_0^1 \mathbf{Z}(\theta')^t \cdot \mathbf{G}(\mathbf{x}_p(\theta')) d\theta' = f + f \langle Z_V \rangle_\theta \Delta I + f \langle \mathbf{Z}_y \cdot \mathbf{P} \rangle_\theta \Delta \mu, \tag{10}$$

where  $f = f(I_0, T_0) = [1 / T_p]$  and  $\langle \cdot \rangle_\theta = \int_0^1 d\theta'$ .

Next,  $f(I_0, T_0)$  can straightforwardly be expanded in  $(\Delta I, \Delta \mu)$ . The quadratic Taylor series is obtained:

$$f(I_0 + \Delta I, \mu_0 + \Delta \mu) = f(I_0, \mu_0) + \frac{\partial f(I_0, \mu_0)}{\partial I} \Delta I + \frac{\partial f(I_0, \mu_0)}{\partial \mu} \Delta \mu + O(\Delta I^2 + \Delta \mu^2). \tag{11}$$

Eqs. (10) and (11) gives us following relational expressions:

$$\frac{\partial f}{\partial I} = f \langle Z_V \rangle_\theta, \tag{12}$$

$$\frac{\partial f}{\partial \mu} = f \langle \mathbf{Z}_y \cdot \mathbf{P} \rangle_\theta. \tag{13}$$

Using Eq. (8),

$$\begin{aligned} \frac{\partial f}{\partial \mu} &= f - f \langle Z_V(Q + I_0) \rangle_\theta \left( \equiv f \left( 1 - \langle Z_V \frac{dV}{d\tau} \rangle_\theta \right) \right) = \\ &= f - f \langle Z_V Q \rangle_\theta - f \langle Z_V \rangle_\theta I_0 = f \left( 1 - \langle Z_V Q \rangle_\theta - \frac{1}{f} \left( \frac{\partial f}{\partial I} \right) I_0 \right). \end{aligned} \tag{14}$$

$[\partial f / \partial \mu] < 0$  is thus satisfied with

$$\langle Z_V Q \rangle_\theta > 1 - \frac{1}{f} \left( \frac{\partial f}{\partial I} \right) I_0.$$

Eq. (14) means that the value of  $[\partial f / \partial \mu]$  is determined by values of  $\langle Z_V Q \rangle_\theta$  and  $[1 - (\partial f / \partial I)(I_0 / f)]$ . It also gives us a condition for frequency transition that  $[\partial^2 f / \partial \mu^2]$  changes from the positive to the negative as  $\mu$  gradually increases via  $\mu = \mu_c$ .  $\mu_c$  represents that  $[\partial f / \partial \mu]$  takes the maximum.

#### IV. SIMULATION RESULT

Using Eq. (14), we systematically investigate frequency characteristics (the frequency decrease and oscillatory transition) of the HH oscillator undergoing a SHCO bifurcation, in terms of  $I$  and  $\mu$ , referring to dynamical mechanisms of a SNIC bifurcation shown in [7].

Firstly, let us explain reasons why frequency decreases, in terms of firing properties in the HH oscillator. Fig.5 shows regions for  $[\partial f / \partial \mu] < 0$  and  $[\partial f / \partial \mu] > 0$  on the  $I-\mu$  phase diagram, being associated with Fig. 4. In Fig. 5,  $(I_{SN}, \mu_{SN}) = (0.16, 0.45)$  classifies a SN bifurcation into two categories: One is the SNIC bifurcation when  $\mu > 0.45$  while the other is the SN bifurcation when  $\mu < 0.45$ . Immediately after SN or SHCO bifurcations,  $[\partial f / \partial \mu] < 0$  is widely occupied in the  $\mu$  range. The range is however rapidly diminished as  $I$  increases. When  $I > 0.26$ , we cannot find any range for  $[\partial f / \partial \mu] < 0$ . This is in a good agreement with changes of the  $f-\mu$  curve in Fig. 4.

Fig. 6(a) shows whether or not  $\langle Z_V Q \rangle_\theta$  is larger than  $[1 - (\partial f / \partial I)(I_0 / f)]$  in Eq. (12) for  $\mu = 1$ , to determine the positive or negative value of  $[\partial f / \partial \mu]$ .  $[\partial f / \partial \mu] < 0$  if  $\langle Z_V Q \rangle_\theta > [1 - (\partial f / \partial I)(I_0 / f)]$ . In contrast,  $[\partial f / \partial \mu] < 0$  if  $\langle Z_V Q \rangle_\theta < [1 - (\partial f / \partial I)(I_0 / f)]$ . Fig. 6(b) represents another evaluation of  $[\partial f / \partial \mu]$  in Eq. (12).  $[\partial f / \partial \mu] > 0$  if  $\langle Z_V \cdot [dV / d\tau] \rangle_\theta < 1$ . To be more precise,  $Z_V \cdot [dV / d\tau]$  for almost all  $\theta$  is greater than 1 at  $I=0.161$ . This can easily expect  $\langle Z_V \cdot [dV / d\tau] \rangle_\theta < 1$  so that  $[\partial f / \partial \mu] < 0$ . However as  $I$  increases from 0.161, the  $\theta$  region that  $Z_V \cdot [dV / d\tau]$  takes greater than 1 is reduced. Thereby,  $\langle Z_V \cdot [dV / d\tau] \rangle_\theta$  is less than 1 so that  $[\partial f / \partial \mu] > 0$ .

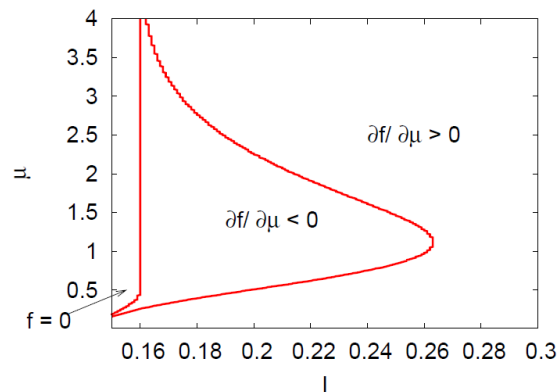


Fig. 5.  $I-\mu$  phase diagram for the class I HH model. The left region show the stationary state of  $f = 0$  while the middle (or right) region shows  $[\partial f / \partial \mu] < 0$  (or  $[\partial f / \partial \mu] > 0$ ). In the diagram, the regions of  $\mu > 0.45$  and  $\mu < 0.45$  are respectively SN and SNIC bifurcations.

Secondly, we confirm a frequency transition of the low to the high level for  $\mu > 6$  and  $I=0.161$  in Fig. 4. For this, we numerically calculate  $[\partial f/\partial \mu]$  as a function of  $I$ . In Fig. 7(a), the  $[\partial f/\partial \mu]$ - $I$  curve has the sharper positive slope,  $[(\partial/\partial I)(\partial f/\partial \mu)] > 0$ , around onsets of oscillations for  $\mu = 5.8$ . However, the curve monotonically decays when  $\mu > 6$ . This implies that the phase transition of the frequency happens. In fact, when  $\mu$  increases at  $I=0.161$ ,  $[\partial^2 f/\partial \mu^2]$  switches from the positive to the negative at  $\mu = \mu_c$  exhibiting  $[\partial^2 f/\partial \mu^2] = 0$ . The peak of the  $[\partial f/\partial \mu]$ - $\mu$  curve is diminished and then disappears for larger  $I$  (Fig. 7(b)). When  $I$  approaches to the bifurcation point ( $I_{SN}$ ), we obtain the following condition for a frequency transition:

$$\lim_{\mu \rightarrow \mu_c^+} \frac{\partial f}{\partial \mu} = +\infty, \quad \lim_{\mu \rightarrow \mu_c^-} \frac{\partial f}{\partial \mu} = +\infty.$$

From bifurcation analysis of Fig. 2(a), let  $\mu$  be  $\mu_c$  when  $V_{SN} = V_{min}(\mu_c)$ . Periodic motions of a trajectory on the LC around  $\mu = \mu_c$  can be described as followings: Membrane potential dynamics immediately before depolarization is extraordinary slow for  $\mu < \mu_c$ , because a trajectory is converge to the LC through the SN equilibrium, thereby leading to a significant phase delay. However when  $\mu > \mu_c$ , a trajectory passes on the LC via the saddle to increase  $[dV/d\tau]$ .

We notice  $[\partial f/\partial \mu] > 0$  after a frequency transition. This is the same result as the HH oscillator undergoing the AH bifurcation [19]. Therefore, we have found that, for any  $I$  in the oscillation range,

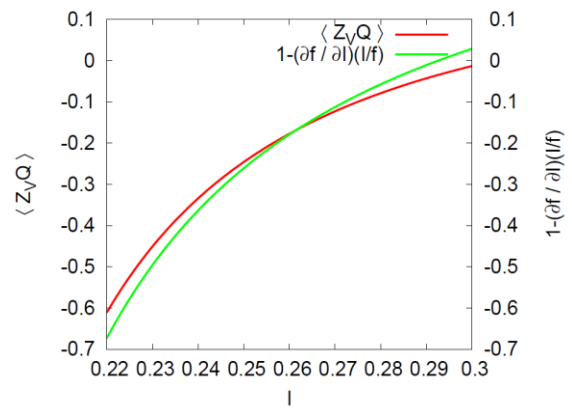
- Class I oscillation:  $[\partial f/\partial \mu]$  takes both the positive and negative values if  $\mu < \mu_c$ , and has the positive value if  $\mu > \mu_c$ .
- Class II oscillation:  $[\partial f/\partial \mu]$  takes the positive value for any  $\mu$ .

### V. DISCUSSION

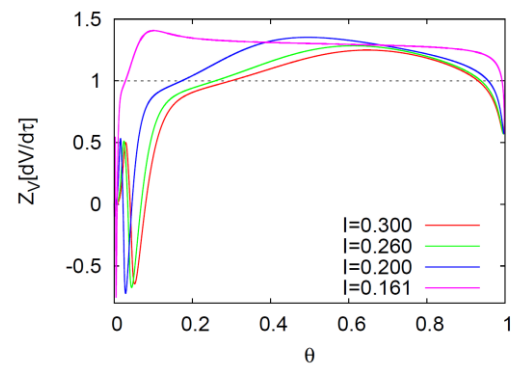
Calculations of  $[\partial f/\partial \mu]$  have ruled out the ambiguity in the conventional classification with different PRC forms, to give clearer classification regardless of the PRC forms. The PRC was traditionally classified into two types: Type I takes almost all positive values for any phase while type II has the obvious negative values as well [20][21]. However, the type I PRC even takes the negative value for extreme narrow phase range and its shape continuously changes to the type II with an increase in  $I$  (as shown in red lines of Fig. 8). There was an open question about definition of the PRC classification.

In comparison with the  $[\partial f/\partial \mu]$  results for the class I, the typical class II  $f$ - $I$  curve has been analyzed by using the original HH neuron that starts oscillations with a finite frequency through the AH bifurcation. The result is only  $[\partial f/\partial \mu] > 0$  for any  $I$  in the oscillation range. We may conclude that, in the class I for the SHCO bifurcation, the  $[\partial f/\partial \mu]$  takes both the positive and negative values, meanwhile  $[\partial f/\partial \mu] > 0$  in the class II for the AH bifurcation.

We have thus shown that computing  $[\partial f/\partial \mu]$  is significantly potential for oscillation classification. One may criticize that the analysis studied here only supports the



(a)



(b)

Fig. 6. (a)  $\langle Z_V Q \rangle_\theta$  (red line) and  $[1 - (\partial f/\partial I)(I_0/f)]$  (green line) represent as functions of  $I$  when  $\mu=1$ . (b)  $Z_V \cdot [dV/d\tau]$  is a function of  $\theta$  ( $\in [0, 1)$ ) at each level of  $I = 0.161, 0.2, 0.26$  and  $0.3$ .

conventional classification with different bifurcation mechanisms of the SN (or SNIC) and AH.

In order to evade such criticism, the two-dimensional Hindmarsh-Rose (2DHR) model, which retains the analytic tractability of the FitzHugh-Nagumo model [22][23], is employed [24]. All bifurcations requested, those being, the AH, the SNIC and the SN are computed in the 2DHR model with appropriate parameter sets. The  $[\partial f/\partial \mu]$ - $I$  curve for each bifurcation is then computed. As the result, the AH, SNIC and SN bifurcations have been categorized into two types:

- Category I ( $[\partial f/\partial \mu] > 0$  and  $[\partial f/\partial \mu] < 0$ ): The SNIC bifurcation.
- Category II ( $[\partial f/\partial \mu] > 0$ ): The AH and SN bifurcations.

As far as we know, the AH and SN bifurcations were not categorized into the same. On the contrary, the SN has so far been regarded to belong to the category for the SNIC bifurcation. In fact, the condition that only  $[\partial f/\partial \mu] > 0$  is showed even if the Terman-Wang (TW) model [25][26] is used [19]. The TW model is one of the analytic tractable neuron models, which generates oscillations via the SN bifurcation.

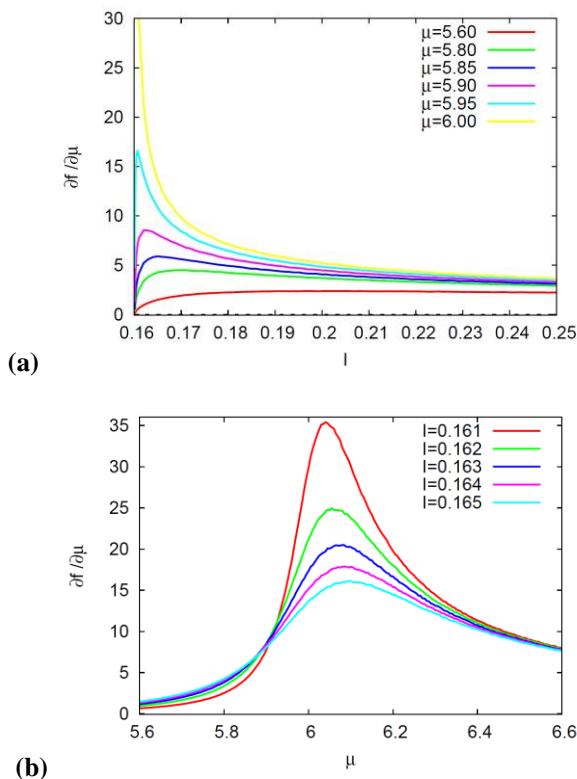


Fig. 7. Results of the Frequency transition when  $\mu > 6$ . (a)  $[\partial f/\partial \mu]-I$  curves when  $\mu=5.6, 5.8, 5.85, 5.9, 5.95$  and  $6.0$ . (b)  $[\partial f/\partial \mu]-\mu$  curves for  $I = 0.161, 0.162, 0.163, 0.164$  and  $0.165$ .

These  $[\partial f/\partial \mu]$  results are supposed to give us important indications about conventional classifications with different bifurcation mechanisms, or different PRC forms. The SN bifurcation that occurs on the LC is crucial for the aforementioned categorization. To be more precise, the necessary condition for  $[\partial f/\partial \mu] < 0$  is that the bi-stability of stable equilibrium and a LC attractor exists. Such a bi-stability cannot be found in the TW model and the 2DHR model exhibiting only stable equilibrium.

Furthermore, the categorization suggested in this work does not address that the PRCs are intensively related to the emergence of oscillations via bifurcation mechanisms. The previous work for class and type classifications [27] indicated that type I PRC has the class I oscillations. This was however no more than an indication at that moment. In Fig. 3(b), the  $f-I$  curve for  $\mu = 0.25$  is the logarithmic class I. Nevertheless, type II PRCs are calculated in any frequency range. As referred to [28] and described in Eq. (5), more precisely, the average of the PRC equals to the slope of the  $f-I$  curves. Therefore, the categorization suggested above is more comprehensive and more sophisticated than the conventional classifications.

The potential task in the near future is to discover some still-unknown oscillatory property of the neuronal circuit undergoing the corresponding bifurcation. Finding novel oscillatory properties allows us to predict bifurcation mechanisms hidden in complex behavior of the neuronal circuit. Since  $[\partial f/\partial \mu]$  is intensively related to  $f-I$  relations as well as PRCs, at least, it can expect to identify bifurcation mechanisms with the more accuracy, compared to only observation of the  $f-I$  relations or PRCs. In the  $f-I$  relations,

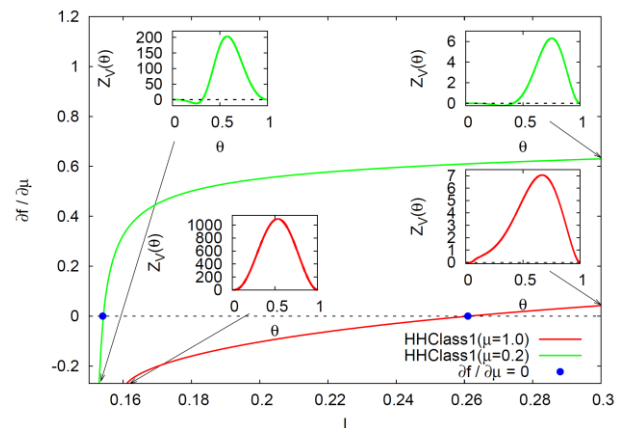


Fig. 8.  $[\partial f/\partial \mu]-I$  curve for  $\mu=1$  (red line) shifts to the one for  $\mu=0.2$  (green line). Correspondingly, the cross point of  $[\partial f/\partial \mu] = 0$  (blue circles) moves so that the  $I$  range for  $[\partial f/\partial \mu] < 0$  is reduced. The PRCs are drawn respectively for  $I = 0.161$  and  $I = 0.3$  when  $\mu=1.0$ , and for  $I = 0.153$  and  $I = 0.3$  when  $\mu=0.2$ .

it is difficult to record at the same time the zero and nonzero frequencies. The PRCs are observed under the environmental noise [29] so that we can difficultly specify bifurcation mechanisms.

Finally, we discuss the temperature scaling factor  $\mu$ . In general, time courses of the ion-channel activations are rescaled with  $\mu = Q_{10}^{(T-T_e)/10}$  with temperature  $T$  °C,  $Q_{10} \sim 3$  and environmental temperature  $T_e$ . In physiological experiments, the temperature is usually fixed around either room temperature or body temperature so that there is not so much temperature variation [5][30]. We may thus have to take care of the temperature parameter to observe stable oscillatory properties of individual neuron corresponding to the recording temperature. Recent model studies are not significantly careful for handling with the temperature parameter [31][32]. In this work, the experimental temperature variation was ignored, because it was crucial and interesting for us to systematically investigate oscillatory properties of the HH model.

## VI. CONCLUSION

We studied a frequency decrease and a frequency transition with a temperature increase in the HH model undergoing SHCO bifurcations. In this study,  $[\partial f/\partial \mu]$  was derived by perturbation analysis of the stable HH oscillators, in combination with  $[\partial f/\partial I]$  and  $(Z_V Q)_\theta$ . We showed that the PRC was clearly classified by  $[\partial f/\partial \mu]$ . More interestingly, different bifurcation mechanisms of the AH and the SN were commonly categorized.

## ACKNOWLEDGEMENTS

The author thanks Natsume and Tateno at Kyushu Institute of Technology and Ikegaya and Aihara at University of Tokyo for fruitful discussions.

## REFERENCES

- [1] C. Lu, Z. Wang, Y. Zhou, and M. Vreugdenhil, Temperature- and concentration-dependence of kainite-induced  $\gamma$  oscillation in rat hippocampal slices under submerged condition, *Acta Pharmacologica Sinica*, 33, 2012, 214-220.
- [2] X.-J. Wang and G. Buzsaki, Gamma Oscillation by Synaptic Inhibition in a Hippocampal Interneuronal Network Model, *J. Neurosci.* 16(20), 1996, 6402-6413.
- [3] M. Yoshioka, Chaos synchronization in gap-junction-coupled neurons, *Phys. Rev. E* 71, 2005, 065203.
- [4] A. Hodgkin and A. Huxley, A quantitative description of membrane current and its application to conduction and excitation in nerve, *J. Physiol.* 117, 1952, 500-544.
- [5] H. A. Braun, M. T. Huber, M. Dewald, K. Schaefer, and K. Voigt, Computer simulations of neuronal signal transduction: the role of nonlinear dynamics and noise, *Int. J. Bifur. Chaos Appl. Sci. Eng.* 8(5), 1998, 881-889.
- [6] U. Feudel, A. Neiman, X. Pei, W. Wojtenek, H. Braun, M. Huber and F. Moss, Homoclinic bifurcation in a Hodgkin-Huxley model of thermally sensitive neurons, *Chaos* 10(1), 2000, 231-239.
- [7] E. M. Izhikevich, *Dynamical Systems in Neuroscience: The Geometry of Excitability and Bursting* (MIT Press, Cambridge, MA, 2007).
- [8] A. Hodgkin, The local electric changes associated with repetitive action in a nonmedulated axon. *J. Physiol.* 107, 1948, 165-181.
- [9] T. Tateno, A. Harsch and H. P. C. Robinson H. P. C. Threshold firing frequency-current relationships of neurons in rat somatosensor cortex: type 1 and type 2 dynamics. *Journal of Neurophysiology*, 92, 2004, 2283-2294.
- [10] Y. D. Sato, K. Okumura, A. Ichiki, M. Shiino and H. Cateau, Temperature-modulated synchronization transition in coupled neuronal oscillators. *Phys. Rev. E*, 85, 2012, 031910.
- [11] E. Dodt and Y. Zotterman, The Discharge of Specific Cold Fibres at High Temperatures; the paradoxical cold. *Acta Physiol. Scand.* 26(4), 1952, 358-65.
- [12] R. R. Long, Sensitivity of cutaneous cold fibers to noxious heat: paradoxical cold discharge. *J. Neurophysiol.* 40(3), 1977, 489-502.
- [13] R. K. Adair, A model of the detection of warmth and cold by cutaneous sensors through effects on voltage-gated membrane channels. *Proc. Natl. Acad. Sci. U S A.* 96(21), 1999, 11825-11829.
- [14] P. Arhem, G. Klement, and C. Blomberg, Channel Density Regulation of Firing Patterns in a Cortical Neuron Model. *Biophys. J.* 90(12), 2006, 4392-4404.
- [15] H. Zeberg, C. Blomberg and P. Arhem, Ion Channel Density Regulates Switches between Regular and Fast Spiking in Soma but Not in Axons. *PLoS Comput. Biol.* 6(4), 2010, e1000753.
- [16] A. Mehrotra and A. Sangiovanni-Vincentelli, *Noise Analysis of Radio Frequency Circuits* (Kluwer, Dordrecht, 2004).
- [17] Y. D. Sato, Synchronization phenomena in a pair of coupled neural oscillators system. *Ph.D. thesis*, Tokyo Institute of Technology, 2005 (unpublished).
- [18] A. Demir, J. Roychowdhury, On the validity of orthogonally decomposed perturbations in phase noise analysis, *Tech Memo* (Bell Labs., Murray Hill, NJ, 1997).
- [19] Y. D. Sato, Neural oscillation classification with temperature-modulated frequency. *Europhys. Lett.* (to be submitted).
- [20] Y. Tsubo, J.-N. Teramae and T. Fukai, Synchronization of excitatory neurons with strongly heterogeneous phase responses. *Phys. Rev. Lett.* 99(22), 2007, 228101.
- [21] Y. Tsubo, M. Takada, A. D. Reyes and T. Fukai, Layer and frequency dependencies of phase response properties of pyramidal neurons in rat motor cortex. *Euro. J. Neurosci.* 25(11), 2007, 3429-3441.
- [22] R. FitzHugh, Impulses and physiological states in theoretical models of nerve membrane. *Biophys. J.* 1, 1961, 445-466.
- [23] R. FitzHugh, Mathematical models of excitation and propagation in nerve, in H.P. Schwan (Ed.), *Biological Engineering*, Chapter 1 (McGraw-Hill Book Co., N.Y. 1969) 1-85.
- [24] S. Tsuji, T. Ueta, H. Kawakami, H. Fujii, K. Aihara, Bifurcations in Two-Dimensional Hindmarsh-rose Type Model. *Int. J. Bifur. Chaos* 17(3), 2007, 985-998.
- [25] D. Terman and D.-L. Wang, Global competition and local cooperation in a network of neural oscillators. *Physica D* 81, 1995, 148-176.
- [26] D.-L. Wang and D. Terman, Locally excitatory globally inhibitory oscillator networks. *IEEE Trans. Neural Net.* 6, 1995, 283-286.
- [27] G. B. Ermentrout, Type I membranes, phase resetting curves, and synchrony. *Neural Comput.* 8, 1996, 979-1001.
- [28] M. A. Schwemmer and T. J. Lewis, Effects of dendritic load on the firing frequency of oscillating neurons. *Phys. Rev. E* 83, 2011, 031906.
- [29] T. I. Netoff, M. I. Banks, A. D. Dorval, C. D. Acker, J. S. Haas, N. Kopell and J. A. White, Synchronization in hybrid neuronal networks of the hippocampal formation. *J. Neurophysiol.* 93(3), 2005, 1197-1208.
- [30] K. S. Cole, R. Guttman and F. Bezanilla, Nerve Membrane Excitation without Threshold. *Proc. Natl. Acad. Sci. U S A.* 65(4), 1970, 884-891.
- [31] Y.-G. Lv and J. Liu, Interpretation on thermal comfort mechanisms of human bodies by combining Hodgkin-Huxley neuron model and Pennes bioheat equation. *Forschung im Ingenieurwesen* 60(2), 2005, 101-114.
- [32] S. Kuang, J. Wang, T. Zeng and A. Cao, Thermal impact on spiking properties in Hodgkin-Huxley neuron with synaptic stimulus. *Pranama* 70(1), 2008, 183-190.